Method for detecting the signature of noise-induced structures in spatiotemporal data sets

M.-Th. Hütt*
Institute of Botany, Darmstadt University of Technology, 64287 Darmstadt, Germany

R. Neff
Institute of Nuclear Physics, Darmstadt University of Technology, 64289 Darmstadt, Germany

H. Busch and F. Kaiser
Institute of Applied Physics, Darmstadt University of Technology, 64289 Darmstadt, Germany
(Received 23 September 2001; revised manuscript received 28 May 2002; published 26 August 2002)

Spatiotemporal stochastic resonance (STSR) is a phenomenon, where the stability of spatial patterns in an extended dynamical system displays a resonance-type dependence on the noise amplitude with the patterns being optimal at intermediate noise level. This dynamical behavior has been found in theoretical systems as well as in biochemical processes, where the noise level has been controlled externally. However, it is an open question how to identify the signature of a spatiotemporal stochastic resonance in a natural system, e.g., in ecology, when the noise amplitude is not known. This question is addressed in the present paper. We provide analysis tools, which allow to reconstruct the noise intensity in a spatiotemporal data set from the data alone. These tools are based on nearest-neighbor considerations inspired by cellular automata and are an appropriate method for detecting STSR, when combined with some measure of spatial order. As a test of our analysis tools, we apply them to sample data generated by four theoretical model systems. We show explicitly that without knowledge of the theoretical value of the noise amplitude for those systems displaying STSR the corresponding resonance curve can be reconstructed from the data alone. In addition, the other (nonresonant) cases are properly identified by our method with no resonance curve being found.

DOI: 10.1103/PhysRevE.66.026117 PACS number(s): 05.40.−a, 07.05.Kf, 87.10.+e, 87.18.Hf

I. INTRODUCTION

The development of new analysis techniques for experimental data can be complemented by studying model systems. This is particularly true for the experimental investigation of nonlinear systems. The idea is to generate sample data using models and then put similar restrictions on these sample data as in the case of an actual experiment. Examples for typical restrictions are (1) only one of the dynamical variable is measured, (2) the sampling rate is reduced, or (3) the values of internal parameters for different time series are unknown.

With the help of such sample data one can test, how well the analysis tools are capable of handling real-life data. In many cases one can improve the analysis techniques significantly on the basis of such tests.

One of the key features of research in nonlinear dynamics is the correspondence between theoretical mechanisms and dynamical processes observed in nature. A prominent example of such a situation is stochastic resonance, where the response of an excitable system to an (e.g., subthreshold) signal is enhanced at intermediate noise levels (for reviews see [1–3]). Similarly to the purely temporal case, where signal transduction reacts resonantly to (external or internal) noise, a spatially extended system can additionally exhibit an enhancement of spatial coherence, called spatiotemporal stochastic resonance (STSR, [4,5]).

A typical restriction when dealing with real experimental data (as opposed to sample data generated with some mathematical model) is ignorance about certain internal parameters of the system: it is one of the main difficulties in finding, e.g., stochastic resonance in natural systems that the value of the noise intensity is frequently not known. This is particularly true for spatiotemporal data, which are currently in the center of interest in biology. Finding such a phenomenon in a natural system can significantly enhance our understanding of the system's functioning [5–7]. However, in some cases sophisticated analysis techniques are necessary to demonstrate the presence of a certain dynamical phenomenon in an experimental data set (see, e.g., Ref. [8] for examples in biology). Spatiotemporal dynamics are particularly difficult to analyze and currently no standardized set of observables exists. Frequent methods are Fourier and wavelet analysis as well as application of image analysis tools [9]. However, image analysis usually focuses on some form of pattern recognition, i.e., a form of data analysis aiming at a very specific situation. Some methods from time series analysis can be generalized to the spatial or spatiotemporal case. For others some straightforward modifications exist to serve the needs of two-dimensional data analysis (see e.g., Refs. [10–12]). The lack of widely applicable quantification methods for spatiotemporal patterns has resulted in a huge amount of quantification attempts, frequently only used for the analysis of a single experiment (see, e.g., Refs. [10,13–15]).

*Corresponding author. Schnittspahnstr.3-5, 64287 Darmstadt, Germany. Electronic address: huett@bio.tu-darmstadt.de

The present article attempts to provide the appropriate tools for searching for STSR in experimental data. We do this in three steps: (1) we introduce the tools themselves (which are spatiotemporal filters based upon nearest-neighbor interactions), (2) we check the performance of these tools using sample data from model systems, some of which display STSR, some of which do not, (3) we discuss some aspects important for the actual application of our tools to real experimental data.

Following this line of thought the structure of our paper is as follows: First we formulate the tools, which are dynamical filters based upon cellular automata considerations (Sec. II). Next we briefly describe (Sec. IV) the theoretical systems, which we used to generate the sample data. Then, as last step, we apply our tools to these model systems in order to extract information on a possible resonance behavior with respect to noise (Sec. V). The advantage is that without using any information on the system other than what would be available as part of an experimental measurement (i.e., in particular without knowledge of the parameters used to generate the data and the value of the noise amplitude) STSR can by reconstructed. The systematics of these results are discussed in Sec. VI.

II. SPATIOTEMPORAL OBSERVABLES AND CELLULAR AUTOMATA

The idea behind cellular automata (CA) is to simulate, which global dynamics of a system result from a certain local interaction [16,17]. Such an interaction is represented in terms of update rules for a cell as a function of its neighborhood. In this general form CA applications may range from the approximate solution of partial differential equations to the study of particles, molecules or biological cells in a local potential generated by their immediate neighbors (see, e.g., Ref. [18,19]). Here our aim is not the study of temporal dynamics after specification of a set of *update rules*, but rather the implementation of local *analysis rules* for a given (experimental or simulated) time development. In this framework the evaluation of a given neighborhood at time t does not yield the state of this particular cell at $t+\Delta t$, but rather gives some characteristic observable for the state of this cell at time t. The state of the automaton is thus translated into a metastate, which shows the observable for each cell corresponding to the analysis rules. This metastate can then be evaluated in different ways. The simplest way of arriving at a definite quantitative measure for the data set at the time t is the summation of all cells with respect to the metastate. Other measures are obtained when the spatial information is retained or additional restrictions are imposed upon the metastate before summation. In this section, we briefly summarize the general idea of such measures and introduce two explicit observables, namely, the CA homogeneity and the CA fluctuation number, both of which have been studied previously in Ref. [20].

Let $\mathcal{I}$ denote a two-dimensional spatial data set, i.e., a square matrix of size N with components $a_{ij}\in\Sigma$, where Σ is the set of possible states. Note that the restriction to a square matrix only refers to the notation used in the text. The observables defined here are applicable to any type of matrices. A time sequence of such matrices or ''images'' is a set

$$\{\mathcal{I}(t);\quad t=1,2,\ldots,N_T\}, \tag{1}$$

where now t denotes some normalized (dimensionless) time and N_T is the number of images in the sequence. The (von Neumann) neighborhood $\mathcal{N}_{ij}$ of an element a_{ij} consists of the element's four nearest neighbors (i.e., for sake of notational convenience in our definition we exclude the central element a_{ij} from the neighborhood).

The first observable to be discussed here is the CA homogeneity. The corresponding analysis rule is given by the mapping

$$a_{ij}\rightarrow\frac{1}{|\mathcal{N}_{ij}|}\sum_{b\in\mathcal{N}_{ij}}\Theta(a_{ij},b), \tag{2}$$

where $|\mathcal{N}_{ij}|$ denotes the number of nearest neighbors b of the cell a_{ij} and the function Θ has to be specified in accordance with the state space Σ as

$$\Theta(a,b)=1-\frac{(a-b)^2}{|\Sigma|^2}, \tag{3}$$

where $|\Sigma|$ is the maximum distance in the state space Σ between two states of cells. In the case of a state space without a distance (e.g., the Ising model, see [20] for details of this analysis) Θ reduces to a δ function, giving 1 for identity and 0 else,

$$\Theta(a,b)=\begin{cases}1, & a=b\\ 0, & a\neq b.\end{cases} \tag{4}$$

We found that the specific form of Θ is not decisive as long as Θ is confined to the interval $[0,1]$ and increases monotonously. Application of Eq. (2) with Θ as in Eq. (3) leads to the metastate of the image $\mathcal{I}$. Normalized summation over all elements in the metastate then gives the CA homogeneity H,

$$H[\mathcal{I}]=\frac{1}{N^2}\sum_{ij}\frac{1}{|\mathcal{N}_{ij}|}\sum_{b\in\mathcal{N}_{ij}}\Theta(a_{ij},b). \tag{5}$$

Here and below all normalization coefficients are written immediately before the corresponding summation. Note that the neighborhood $\mathcal{N}_{ij}$ of cells at the boundaries has to be modified according to the boundary conditions. In a system, where the average value over all cells changes significantly with time, an appropriate measure of spatial order is the difference between the actual homogeneity $H[\mathcal{I}]$ and a state homogeneity $H_S[\mathcal{I}]$ given by

$$H_S[\mathcal{I}]=\sum_{a,b\in\Sigma}\Theta(a,b)p_a p_b, \tag{6}$$

with the probability p_x of the state $x\in\Sigma$ and the function Θ from Eq. (4). Equation (6) is the expectation value of $\Theta(a,b)$ over the whole spatial lattice. One can think of the quantity H_S as the average homogeneity obtained by reshuf-

fling all cells and, thus, destroying spatial order. In the following, the resulting *reduced homogeneity*

$$h[\mathcal{I}]=H[\mathcal{I}]-H_S[\mathcal{I}] \tag{7}$$

is used, rather than the homogeneity $H[\mathcal{I}]$ itself. It is shown below that for the choice of Θ as in Eq. (3) this difference $h[\mathcal{I}]$ is proportional to the covariance of a matrix $\mathcal{I}$. Even for small spatiotemporal data sets this method of calculating a quantity describing the spatial correlation is fast and reliable.

$H[\mathcal{I}]$, $H_S[\mathcal{I}]$, and $h[\mathcal{I}]$ of Eqs. (5), (6), and (7), respectively, can be related to commonly used statistical properties. Defining the variance V of an image $\mathcal{I}$ as

$$V[\mathcal{I}]=\frac{1}{N^2}\sum_{ij}(a_{ij}-\overline{a})^2=\overline{a^2}-\overline{a}^2, \tag{8}$$

where

$$\overline{a}=\frac{1}{N^2}\sum_{ij}a_{ij}, \quad \overline{a^2}=\frac{1}{N^2}\sum_{ij}a_{ij}^2, \tag{9}$$

and the purely spatial autocovariance χ_1 of nearest neighbors for the image $\mathcal{I}$ as

$$\begin{aligned}\chi_1[\mathcal{I}]&=\frac{1}{N^2}\sum_{ij}\frac{1}{|\mathcal{N}_{ij}|}\sum_{b\in\mathcal{N}_{ij}}(a_{ij}-\overline{a})(b-\overline{a})\\&=\frac{1}{N^2}\sum_{ij}\frac{1}{|\mathcal{N}_{ij}|}\sum_{b\in\mathcal{N}_{ij}}(a_{ij}b-\overline{a}^2),\end{aligned} \tag{10}$$

one finds for H

$$\begin{aligned}H[\mathcal{I}]&=\frac{1}{N^2}\sum_{ij}\frac{1}{|\mathcal{N}_{ij}|}\sum_{b\in\mathcal{N}_{ij}}\left(1-\frac{(a_{ij}-b)^2}{|\Sigma|^2}\right),\\&=1-\frac{2}{|\Sigma|^2}\left(V-\frac{1}{N^2}\sum_{ij}\frac{1}{|\mathcal{N}_{ij}|}\sum_{b\in\mathcal{N}_{ij}}(a_{ij}b-\overline{a}^2)\right),\end{aligned}$$

and, therefore,

$$H[\mathcal{I}]=1-2\frac{V[\mathcal{I}]-C_1[\mathcal{I}]}{|\Sigma|^2}, \tag{11}$$

where the autocorrelation coefficient C_1 is defined as

$$C_1=\frac{\chi_1[\mathcal{I}]}{V[\mathcal{I}]}. \tag{12}$$

This demonstrates that the CA homogeneity H is a universal measure abstracting from the specific properties of the analyzed system. The state homogeneity H_S from Eq. (6) can be written as

$$H_S[\mathcal{I}]=\frac{1}{N^4}\sum_{ij}\sum_{kl}\left(1-\frac{(a_{ij}-a_{kl})^2}{|\Sigma|^2}\right)=1-\frac{2V[\mathcal{I}]}{|\Sigma|^2}. \tag{13}$$

So the reduced homogeneity $h[\mathcal{I}]$,

$$h[\mathcal{I}]=H[\mathcal{I}]-H_S[\mathcal{I}]=2\frac{C_1[\mathcal{I}]}{|\Sigma|^2}, \tag{14}$$

is proportional to the autocovariance of the image $\mathcal{I}$ and gives the complete spatial information about neighbor sites within $\mathcal{I}$. Note that this relation is only valid for the particular form of Θ from Eq. (3).

Noise and fluctuations can be thought of as the contribution of processes with small time constants in the observed dynamics [21]. This prerequisite in mind, we assume that the fluctuations under consideration enter the model systems as white or nearly δ-correlated noises.

The key idea here for quantification of such contributions is to use the relative movement of neighbors of a particular cell $a_{ij}^{(t)}$ at a time t, i.e., changes of the quantities $\delta_{ij}^{(t,k)}$ in

$$\delta_{ij}^{(t)}=\{a_{ij}^{(t)}-b^{(t)};\quad b^{(t)}\in\mathcal{N}_{ij}\}=\{\delta_{ij}^{(t,1)},\ldots,\delta_{ij}^{(t,|\mathcal{N}_{ij}|)}\},$$

as a means of separating directed and undirected (eventually stochastic) change of the state of a cell. If the discretization of the spatiotemporal data set in space (due to the finite cell size) and time (due to the finite number of images) is small enough, directed and stochastic changes will have very different scales in time and space.

For means of separation, one has to assume that the scales for the stochastic part will be smaller than the scales present in the discretization of the data set and the time scales of deterministic dynamics themselves (cf. the Appendix).

This leads to a (sufficient) condition for a manifestation of noise in a specific change at $a_{ij}^{(t)}$,

$$\begin{aligned}&\mathrm{Sig}[\,\delta_{ij}^{(t,k)}-\delta_{ij}^{(t-1,k)}]\neq\mathrm{Sig}[\,\delta_{ij}^{(t+1,k)}-\delta_{ij}^{(t,k)}]\\&\wedge\,\delta_{ij}^{(t,k)}-\delta_{ij}^{(t-1,k)}\neq 0\quad\wedge\,\delta_{ij}^{(t+1,k)}-\delta_{ij}^{(t,k)}\neq 0,\end{aligned} \tag{15}$$

where the last two inequalities are subsidiary conditions introduced for convenience and the sign function

$$\mathrm{Sig}[x]=\begin{cases}+1, & x>0\\ 0, & x=0\\ -1, & x<0\end{cases}$$

has been used. Each transition $\delta_{ij}^{(t-1,k)}\to\delta_{ij}^{(t,k)}\to\delta_{ij}^{(t+1,k)}$ fulfilling the condition (15) gives a contribution

$$\frac{1}{2}(|\,\delta_{ij}^{(t,k)}-\delta_{ij}^{(t-1,k)}|+|\,\delta_{ij}^{(t+1,k)}-\delta_{ij}^{(t,k)}|). \tag{16}$$

Averaging with respect to k,i, and j leads to the final expression for the CA fluctuation number $\Omega(t)$,

$$\Omega(t)=\frac{1}{N^2}\sum_{ij}\frac{1}{|\mathcal{N}_{ij}|}\sum_{k=1}^{|\mathcal{N}_{ij}|}\frac{1}{2}(|\delta_{ij}^{(t,k)}-\delta_{ij}^{(t-1,k)}| + |\delta_{ij}^{(t+1,k)}-\delta_{ij}^{(t,k)}|)\frac{1}{2}\mathrm{Sig}[\delta_{ij}^{(t,k)}-\delta_{ij}^{(t-1,k)}] \times \mathrm{Sig}[\delta_{ij}^{(t+1,k)}-\delta_{ij}^{(t,k)}](\mathrm{Sig}[\delta_{ij}^{(t,k)}-\delta_{ij}^{(t-1,k)}] \times \mathrm{Sig}[\delta_{ij}^{(t+1,k)}-\delta_{ij}^{(t,k)}]-1), \quad (17)$$

where the term in the second row is either 0 or 1 filtering the dynamics according to the fluctuation condition (15). In the following, we will show that the quantity Ω in combination with the reduced homogeneity h or with the (nearest-neighbor) correlation coefficient of the image $\mathcal{I}$ is capable of distingushing between STSR and a nonresonant behavior with respect to noise.

III. APPLICATION TO EXPERIMENTAL DATA

A well-designed experiment for spatiotemporal dynamics will yield data with a higher spatial (and temporal) resolution than required by the dynamics of the system.

This, however, means that one does not automatically apply these tools to the appropriate length scale. Tha CA homogeneity, for example, when naively applied to a time series of high-resolution spatial images will be dominated by measurement noise, rather than quantifying the patterns arising on the level of the system's dynamics. In such cases it is necessary to study the *scale dependence* of the observables.

In the case of experimental data analyzing this scale dependence is straightforward: one has to substitute blocks of $s\times s$ pixels, each containing the numerical measurement value, by their average value. Such a *binning* yields a spatial image with a lower resolution for which, e.g., the CA homogeneity H can be calculated. Averaging over time and varying s one obtains H as a function of the scale s.

On the other hand, a lot can be learned about the length scales present in the experimental data, when one, in principle, knows what behavior of the observables one can expect. Then the scale dependence of these observables can help to extract characteristic scales of different contributions to the dynamics, even if some of them are masked by measurement noise or more than one length scale is present in the system. A detailed analysis of the scale-dependence for ''data'' generated by theoretical model systems has been performed in [22].

In addition to binning, some application of noise-reduction techniques may be an appropriate preparation of the experimental data before studying them with the tools described in the preceding section.

The CA homogeneity can often be substituted by standard tools for the quantification of clustering phenomena. In the following we will show this explicitly for the spatial correlation coefficient. In Ref. [20] the CA homogeneity has also been compared with cluster quantification algorithms.

In practice any application of these spatiotemporal filters can be (and often has to be) complemented by further data analysis techniques, such as stationary tests and methods based on surrogate data.

IV. THEORETICAL MODELS USED TO GENERATE SAMPLE DATA

In this section, we apply the observables defined above to four different theoretical model systems, each of which is a network of coupled nonlinear oscillators. The individual units are FitzHugh-Nagumo oscillators, Sel'kov oscillators, Braaksma-Grassman oscillators, and a threshold device leading to a CA-type excitable medium introduced in Ref. [4] and further studied in Ref. [23]. While the first two systems are well known, the latter two require some comment. The Braaksma-Grassman system (see, e.g., [24,25]) is an externally driven network of excitable oscillators in which stochastic resonance has recently been found [25]. The system from Ref. [4], which in the following we will refer to as the Jung system, is an excitable media cellular automaton with a threshold and an exponentially decaying coupling between elements. The explicit forms of the model systems are as follows.

(1) FitzHugh-Nagumo (FHN): The model is given by (see, e.g., Ref. [26])

$$\dot{u}_{ij}=[(a-u_{ij})(u_{ij}-1)u_{ij}-v_{ij}]\frac{1}{\epsilon}+\xi_{ij}(t)+D\Delta u_{ij},$$

$$\dot{v}_{ij}=bu_{ij}-\gamma v_{ij}-c \quad (18)$$

with parameters $(a,b,c,\gamma,\epsilon,D)=(0.15,0.0024,0.0,0.003,1.0,0.05)$ in the excitatory regime and the diffusion term

$$\Delta u_{ij}=\sum_{kl\in\mathcal{N}_{ij}}(u_{kl}-u_{ij}). \quad (19)$$

The neighborhood $\mathcal{N}_{ij}$ consists of the four nearest neighbors of the element (ij). For the discussion of the oscillatory regime we use the following parameter values: $(a,b,c,\gamma,\epsilon,D)=(0.5,1.0,0.3,0.5,0.01,0.1)$.

(2) Sel'kov (oscillatory): We use the following form of the Sel'kov system [27]:

$$\dot{u}_{ij}=-u_{ij}+\lambda v_{ij}+v_{ij}u_{ij}^2,$$

$$\dot{v}_{ij}=b-\lambda v_{ij}-v_{ij}u_{ij}^2+\xi_{ij}(t)+D\Delta v_{ij} \quad (20)$$

with parameters $(b,\lambda,D)=(0.66,0.114,0.16)$ and a coupling term Δv_{ij} corresponding to the one given in Eq. (19).

(3) Braaksma-Grassman (BG) (excitatory): The BG system is given by

$$\epsilon\dot{u}_{ij}=v_{ij}-\frac{1}{2}u_{ij}^2-\frac{1}{3}u_{ij}^3,$$

$$\dot{v}_{ij}=\alpha-u_{ij}+\xi_{ij}(t)-Du_{ij} \quad (21)$$

with parameters $(\alpha,\epsilon,D)=(0.1,0.01,0.15)$ and a coupling term as in Eq. (19). The system is driven by an external force

$A\cos(\omega t)$ with $A=1$ and $\omega=18$ [time units (t.u.)]$^{-1}$ acting additively upon the v_{ij} with $i=1,1\leqslant j\leqslant 32$.

Due to the negative sign of the coupling constant D in Eq. (21), coupled neighbors are driven in opposite directions. For optimal coupling and noise the oscillators drive each other into the stationary or excited state in a temporally and spatially alternating fashion. Because Eq. (21) has no back coupling, excitations can propagate only in one direction. Hence, in the resonant state plane waves propagate according to the unidirectional coupling across the system, while direct neighbors oscillate in an antiphase manner and every second element pulses in phase. This results in a checkerboardlike pattern [cf. Fig. 2(a), system 2]. Decreasing or increasing the noise level destroys simple geometrical patterns as the system becomes less excited [Fig. 2(a), system 1 and 3] or noise dominated (system 4), respectively.

(4) Jung CA: The Jung CA has been implemented as described in Ref. [4]. We investigate a 100×100 grid of pulse-coupled threshold devices, whose time evolution is given by

$$u_{ij}(t+\Delta t)=(1-\gamma)u_{ij}(t)+\xi_{ij}(t)+D_{ij} \tag{22}$$

with spatially incoherent Gaussian noise ξ_{ij} and a dissipation parameter $\gamma=0.5$. A network element fires when it crosses a threshold value of 1.0, after which it enters a refractory period of nine time steps, during which it cannot be excited again. The coupling D_{ij} regulates the contribution to x_{ij} from input of all other elements in the network that fire at time $t-\Delta t$.

$$D_{ij}=K\sum_{kl}\ \exp\left(-\lambda\frac{r_{ij,kl}^2}{a^2}\right), \tag{23}$$

where $r_{ij,kl}^2$ is the squared Euclidian distance between communicating elements normalized to the grid spacing $a=1.1$. The spatial decay of the coupling is given by $\lambda=0.1$ The quantity $K=0.176$ is the coupling strength.

Networks of 32×32 oscillators with randomized initial conditions have been simulated. Only for the Jung system a network of 100×100 elements is discussed. We applied open boundary conditions for the excitatory FHN system, the BG system and the Jung system, while for the Sel'kov and the oscillatory FHN systems periodic boundary conditions have been used.

In all cases the numerical simulations have been carried out using exponentially correlated, colored noise, which provides a more realistic description of real fluctuations in biological systems, as compared to spectrally flat noise. It is generated by an Ornstein-Uhlenbeck process (see Ref. [25] and references given there). The noise intensity σ^2 is defined via the standard deviation of the Gaussian-distributed noise amplitudes,

$$\langle\xi(t)\rangle=0, \tag{24}$$

$$\langle\xi(t)\xi(t')\rangle=\frac{\sigma^2}{\tau_c}\exp\left(-\frac{|t-t'|}{\tau_c}\right), \tag{25}$$

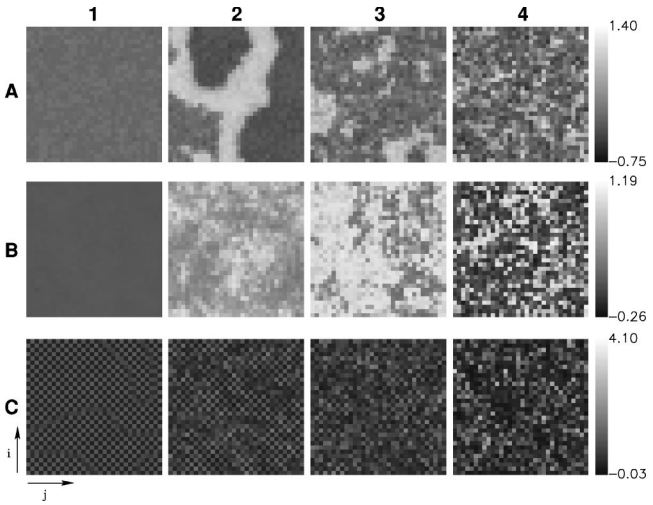

FIG. 1. Snapshots of the typical dynamical behavior of two of the model systems. The state of one dynamical variable (as described in the text) is shown for four different noise intensities σ^2. (a): FHN system in its excitatory regime (the values of σ^2 are $1{:}9\times 10^{-5}$, $2{:}3\times 10^{-4}$, $3{:}1\times 10^{-3}$, $4{:}8\times 10^{-3}$), (b): FHN in the oscillatory regime ($1{:}2\times 10^{-4}$,$2{:}2\times 10^{-3}$,$3{:}2\times 10^{-2}$,$4{:}1\times 10^{-1}$), (c): Sel'kov system ($1{:}1\times 10^{-3}$,$2{:}2.4\times 10^{-2}$,$3{:}0.05$, $4{:}0.25$). In all cases an array of 32×32 oscillators has been used. The parameter values are given in Sec. IV.

where τ_c is the noise correlation time. The noise term $\xi_{ij}(t)$ is uncorrelated from site to site, i.e., spatially incoherent. Equations (18–21) were numerically integrated using a Heun algorithm [28] with a stepsize $\Delta t=10^{-3}$ t.u. The noise correlation time has been chosen to be $\tau_c=10^{-3}$ t.u.

Throughout this paper, the model parameters are held constant, except for the noise intensity σ^2. We checked, however, that the forms of dynamics discussed here persist over a wide range of the model parameters.

V. RESULTS

Even with the eye one sees significant differences between the snapshots at different noise intensities for each of the four systems shown in Figs. 1 and 2. A quantitative analysis, however, is not straightforward, in particular, when the noise intensity itself is not given as an additional information.

Note that here and in the following we use only one of the dynamical variables to quantify spatial organization. This is closer to the case of real experimental data, as in most cases only one of the system's dynamical variables is observed. We used the variable u for all systems studied here. For the first two cases (excitatory and oscillatory FHN) we will give four diagrams, namely, the reduced homogeneity $h(\sigma^2)$, the CA fluctuation number $\Omega(\sigma^2)$, a correlation diagram with pairs (h,Ω), and a correlation diagram with pairs (C_1,Ω), where C_1 is the spatial nearest-neighbor correlation coefficient (i.e. the usual autocorrelation coefficient) of the image $\mathcal{I}$. For the other systems only the correlation diagram of pairs (h,Ω), is given, as in these cases the quantity C_1 showed the same qualitative behavior as h and, thus, did not provide any ad-

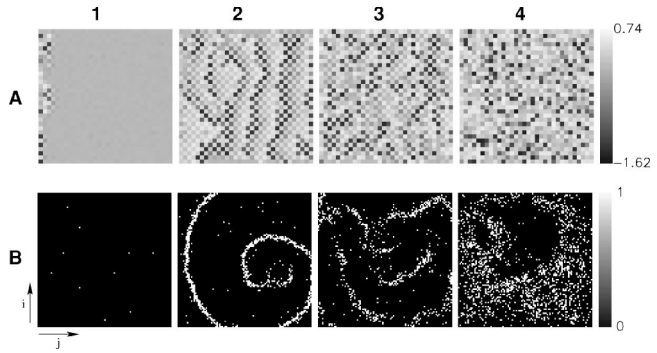

FIG. 2. Snapshots of the typical dynamical behavior of the remaining two model systems. As in Fig. 2 the state of one dynamical variable is shown for four different noise intensities. (a): BG system (the values of σ^2 are $1{:}1\times10^{-5}$, $2{:}1\times10^{-4}$, $3{:}8\times10^{-4}$, $4{:}5\times10^{-3}$), (b): Jung system (1:0.07,2:0.10,3:0.15,4:0.35). Again, the parameter values are given in Sec. IV.

ditional information. In all cases averages over many time steps have been taken (see figure captions for details) and a transient at the beginning of each time series has been skipped.

Figure 3(a) shows the reduced homogeneity $h=H-H_S$ as a function of the noise intensity σ^2 for the FHN system in the excitatory regime. A resonance-type behavior is seen with a maximum around $\sigma^2\approx0.0006$. An important intermediate step in our attempt to recover the stochastic resonance from the ''data'' set alone is given in Fig. 3(b), where the CA fluctuation number Ω is shown as a function of σ^2. Due to the monotonous, over a wide range of σ^2 almost linear, shape of the curve, Ω is able to quantify the inherent noise intensity. Thus, we are now able to obtain the resonance curve solely from information present in the data sets themselves. This is shown in Fig. 3(c), which is a scatter plot (or correlation diagram) of the pairs (h,Ω). At this stage of the analysis process information on the theoretical noise intensity σ^2 is no longer necessary. In this manner our analysis technique could also be applied to real (i.e., not artificial) data, e.g., when dealing with ecosystem dynamics or in vivo systems, where no direct information of the noise intensity is available. The second correlation diagram, Fig. 3(d), displaying the correlation coefficient C_1 together with the CA fluctuation number Ω confirms this picture. Here the resonance is even more clearly visible.

The response of the system to noise changes visibly, when one passes to the oscillatory regime of the FHN system. Figure 4 shows the corresponding results of our analysis. From the snapshots in Fig. 1(b) it can be seen that one no longer finds stable patterns at intermediate noise intensities. However, the average size of clusters still seems to depend on the noise intensity in a nonmonotonous way. This impression is captured by the reduced homogeneity [Fig. 4(a)], where a peak in $h(\sigma^2)$ is seen around $\sigma^2\approx0.01$. In this case, the σ^2 dependence of the correlation coefficient C_1 deviates from that observed for the function $h(\sigma^2)$, as for C_1 no resonant behavior is found [cf. Fig. 4(d)]. The effect is much less dramatic, however, than in the excitatory case, where the resonance was also observed in the noise dependence of the correlation coefficient, Fig. 3(d). Nevertheless, on the basis of Fig. 4(a), which corresponds to what is seen in the snapshots from Fig. 1(b), we find that a measure of spatial order shows a resonance-type dependence on the noise intensity.

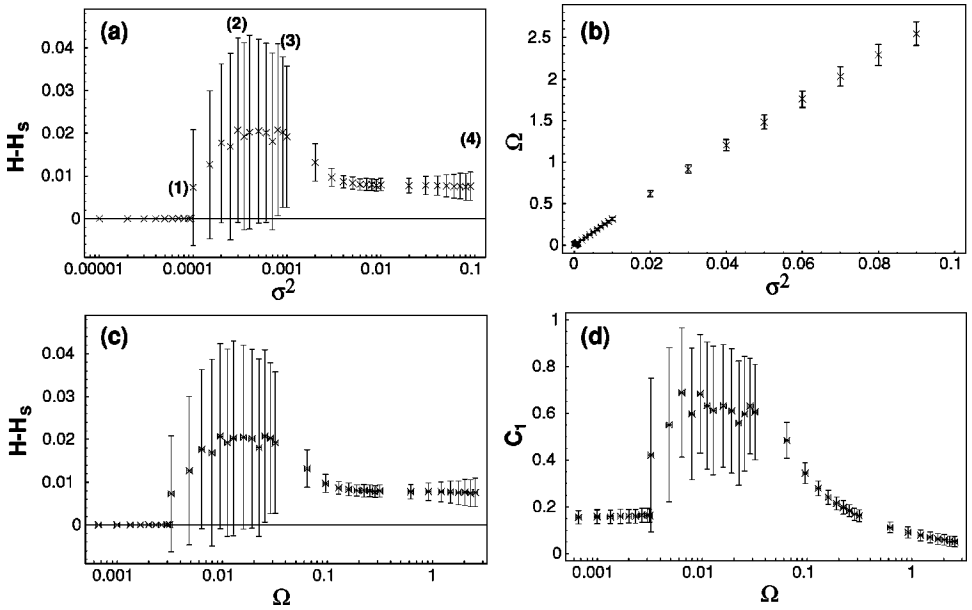

FIG. 3. The dependence of the reduced homogeneity $h=H-H_S$ [cf. Eq. (7)] on the noise amplitude σ^2 for a lattice of FHN oscillators in the excitatory regime (a). For the computation of h an average over 3500 time series samples with a sampling rate of 10 t.u.$^{-1}$ has been taken. For parameter values see the discussion in Sec. IV. Panel (b) shows the dependence of the CA fluctuation number Ω [cf. Eq. (17)] on the noise intensity σ^2. In panel (c) the correlation diagram of h and Ω. The shape of the curve in panel (a) is retained. The numbers in brackets shown in the panel (a) indicate the noise intensities at which the snapshots in Fig. 1 have been taken. Panel (d) gives the correlation diagram of the correlation coefficient C_1 and the CA fluctuation number Ω.

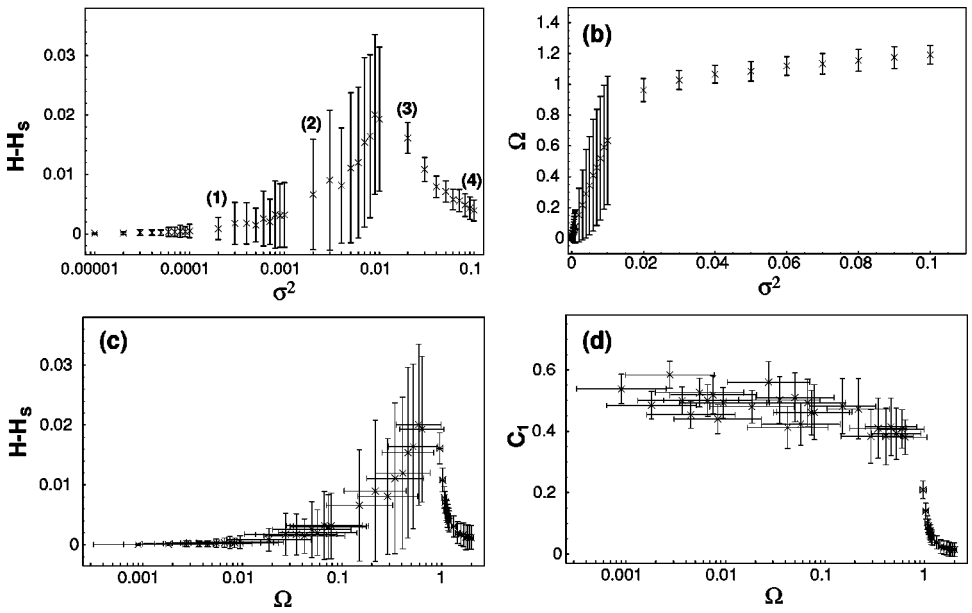

FIG. 4. Same as Fig. 3, but for the FHN system in the oscillatory regime. The average has been taken over 500 samples with a sampling rate of 5 t.u.$^{-1}$. Both, panel (a), which contains the theoretical noise intensity, as well as panel (c), where the noise intensity reconstructed with the fluctuation number has been used, show some evidence of STSR. In the correlation diagram (d) of pairs (C_1,Ω) no resonant behavior is seen.

This can also be seen as a special case of STSR. As before, the function $\Omega(\sigma^2)$ shows a monotonous behavior, but the two distinct regimes discernable in Fig. 4(b) lead to a shift of the peak in the correlation diagram, Fig. 4(c). The correlation coefficient C_1 remains almost constant over a wide range of σ^2 and then sharply decreases at high σ^2 [cf. the correlation diagram shown in Fig. 4(d)]. Thus, even without knowledge of the noise intensity, we can reproduce the evidence for this form of STSR found in Fig. 4(a).

The results for the Sel'kov system are shown in Fig. 5. As the correlation coefficient C_1 and the reduced homogeneity h display qualitatively the same dependence on σ^2 we only show the corresponding results for h. In accordance with what is expected from the snapshots shown in Fig. 1(c), we find no STSR for the (oscillatory) Sel'kov system. The reduced homogeneity h changes sign with increasing σ^2, but no resonance is found. Again, the almost linear relation between Ω and σ^2 seen in Fig. 5(b) allows us to rely on the data alone for reproducing the noise dependence of the reduced homogeneity in terms of a correlation diagram showing pairs (h,Ω) [Fig. 5(c)].

In Ref. [25] Busch and Kaiser have quantified the phenomenon of STSR for the BG system by studying the average number of oscillators within each column of the array that are spiking within a short time interval as a function of the noise amplitude σ. The resulting observable is optimal for this particular type of oscillation patterns, but is difficult to transfer to other dynamical systems. Here we use the reduced homogeneity as an alternative. As is seen in Fig. 6 this is sufficient to obtain a similar resonance-type structure as in the case of the quantity used in [25]. Due to the anticorrelation of neighboring oscillators [cf. the snapshots shown in Fig. 2(a)] the reduced homogeneity h, being based on nearest-neighbor considerations, decreases with more and more ordered plane waves running through the lattice. Hence, h as a function of the theoretical noise intensity σ^2 shows a minimum in Fig. 6(a) around $\sigma^2\approx 0.009$. At that point the average number of oscillators spiking synchronously within each column has a maximum (cf. [25]).

Already from the snapshots [Fig. 2(c)] for the Jung system one can appreciate the fact that noise intensity regulates the structural stability of the spiral waves appearing in this excitable medium. The reduced homogeneity $h=h(\sigma^2)$ has a sudden increase at about $\sigma^2\approx 0.09$ and shows a maximum around $\sigma^2\approx 0.11$ followed by a slow descent at higher σ^2 [cf. Fig. 7(a)]. Although the CA fluctuation number Ω also shows a pronounced jump at $\sigma^2\approx 0.09$, it nevertheless is a monotonous function of σ^2 [cf. Fig. 7(b)]. Consequently, the resulting correlation diagram, Fig. 7(c) correctly identifies the system's behavior as STSR.

VI. DISCUSSION

We introduced a method for quantifying spatiotemporal dynamics in spatially and temporally discrete systems under the influence of noise. The capabilities of the method are illustrated here by applying it to a data set with a known mechanism of generation and, thereby, detecting spatiotemporal stochastic resonance displayed by some of the model systems.

With the help of this method, we found STSR in the excitatory FHN system, in the BG system and in the Jung system. Some evidence for STSR has been found in the oscillatory FHN system. The Sel'kov system showed no resonant behavior with respect to noise intensity. All these results could be reproduced without knowledge of the noise intensity by studying correlation diagrams of some spatial observable (in our cases the reduced homogeneity or the spatial correlation coefficient) with the CA fluctuation number introduced in Sec. II.

It is clear, however, that a lot of detailed studies are necessary in order to see, how this method deals with situations, which are not as standard as the system investigated here. The crucial ingredient is the monotonous behavior of the CA fluctuation number Ω as a function of σ^2. We have tested the

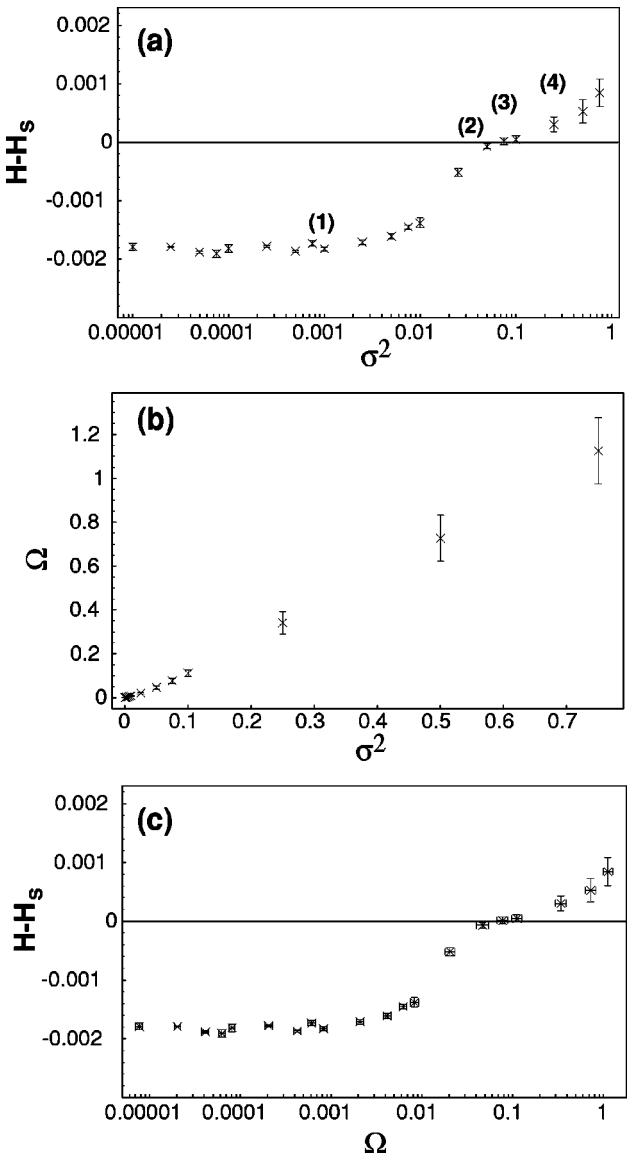

FIG. 5. Same as Figs. 3(a)–3(c), but for the Sel'kov system. The average has been taken over 500 samples with a sampling rate of 10 t.u.$^{-1}$. Now only one correlation diagram is shown, namely of pairs (h,Ω). No evidence for STSR is found.

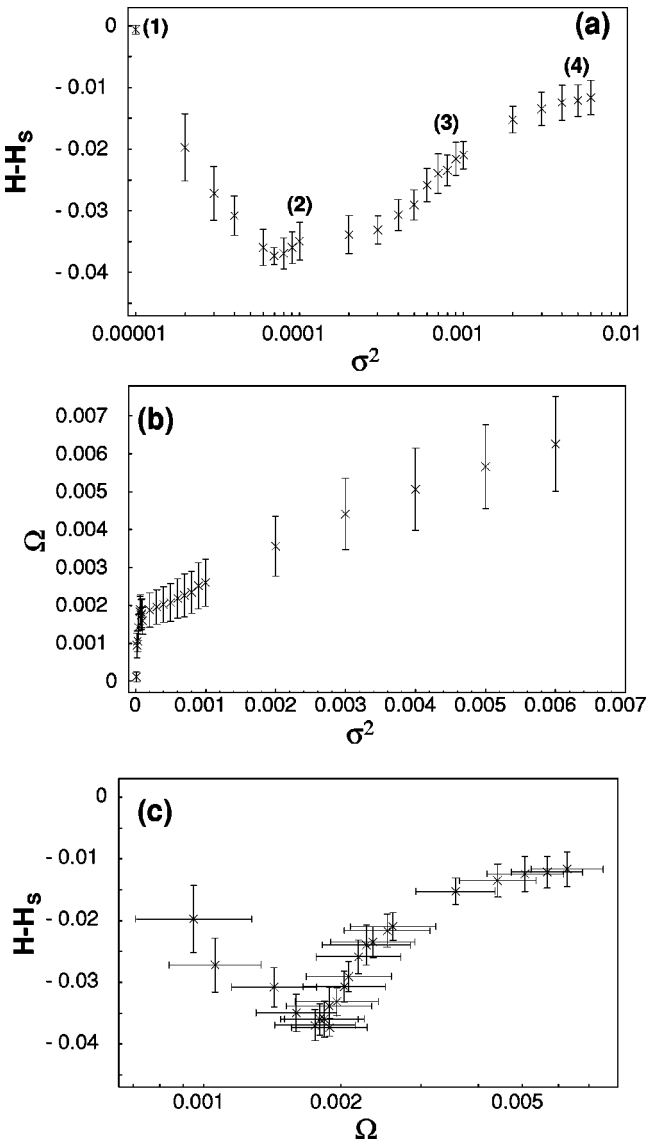

FIG. 6. Same as Fig. 5, but for the system of BG oscillators, with the time average taken over 500 samples with a sampling rate of 10 t.u.$^{-1}$. A minimum occurs around $\sigma=0.008$. The system's most ordered state is perfectly anticorrelated (cf. the snapshots in Fig. 2 and the discussion in Sec. IV). Thus, the signature of STSR in this case is a minimum of $h(\sigma)$.

fluctuation number Ω quantifying successfully the noise intensity in several theoretical systems. A universal formulation of the conditions under which Ω is a monotonous function of the (internal) noise level of the system has not yet been achieved.

A major difference between real spatiotemporal data sets and the examples given here is the existence of a canonical length and time scale in the image sequences of the model systems. The spatial and temporal resolution of the experimental data usually is much higher than the typical length and time scales present in the system and, therefore, nearest-neighbor considerations might be difficult to apply. In practice, it may thus become necessary to scale the spatial data points, as described in Sec. III, before using the definitions given in the present paper. Currently we are applying our methods to a variety of experimental data, e.g., to the analysis of vegetation patterns in extended ecological systems and to chlorophyll fluorescence images of plant leaves (see Ref. [29] for examples of the experimental data for the latter case).

The rationale behind these applications is that whenever an observable quantifying spatial structure displays a resonance in the correlation diagram with the CA fluctuation number, this can be regarded as evidence for STSR.

Several important questions have not been addressed here. It would, for example, be useful to have some means of deciding, whether a given data set fulfills the conditions for application of our method, particularly the scale of discretization in space and time. In practice, however, one often has

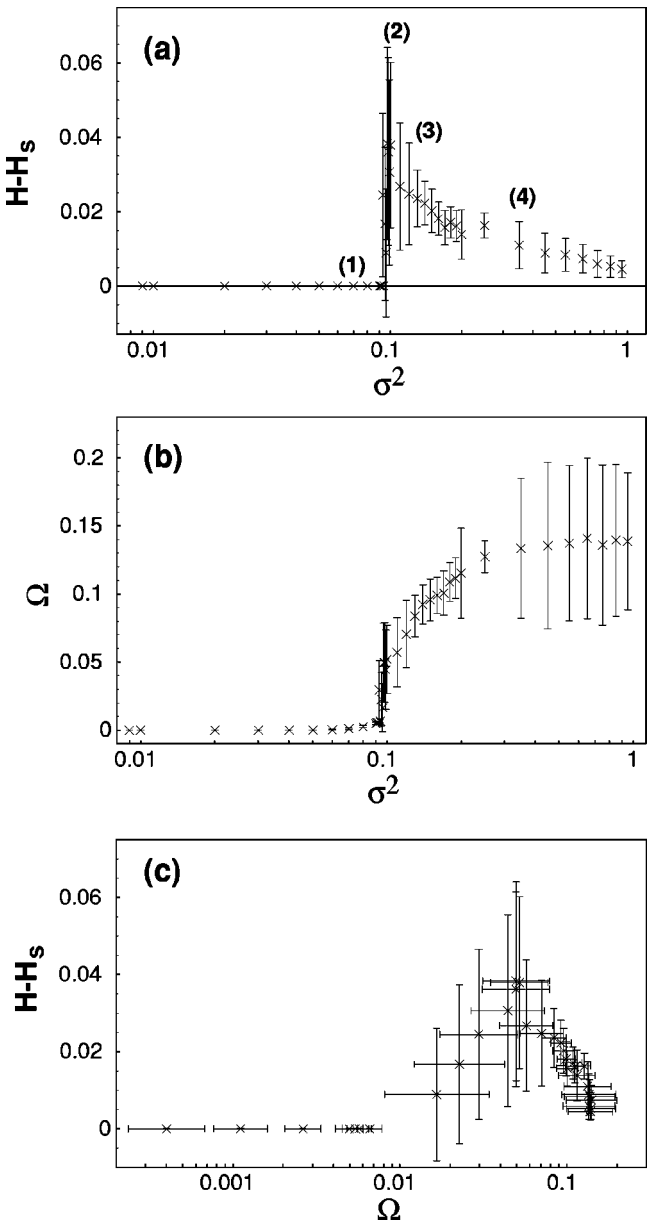

FIG. 7. Same as Fig. 5, but for the Jung system, now with an average over 260 samples, sampling at every other time step. The maximum in h is the signature of STSR.

additional information about the system (e.g., about typical length scales or time constants), which can be used to clarify this point. In any case, it is useful to study the stability of the results under variation of the discretization scale in space and time. This can be done both experimentally (by changing, if possible, the resolution of the experimental setup) or theoretically (by introducing some binning before extracting the observables).

As pointed out, a second question not discussed in depth here concerns the conditions for the monotonous relation between noise intensity σ and CA fluctuation number Ω as mentioned above. The analytical material of the appendix may help to gain access to this property of Ω, without, however, solving the full mathematical problem. Clearly, a rigorous result would facilitate application to real experimental data.

The development of methods for extracting characteristic and useful information on spatiotemporal phenomena from experimental data is still at its beginning. The principal aim is to formulate standardized analysis methods, which are tested and gauged by applying them to theoretical systems and by examining the correlation with existing observables. With the present paper, we have tried to provide some ideas in this direction.

ACKNOWLEDGMENTS

The authors are indebted to F. Beck, A. Bohn, and U. Lüttge for useful discussions. Support was provided by the Deutsche Forschungsgemeinschaft, Bonn/Germany, within the framework of Sonderforschungsbereich 199 (Teilprojekt B5) and Graduiertenkolleg 340.

APPENDIX

An analytical interpretation of the CA fluctuation number Ω (Eq. 17) can be obtained in the following way: The contribution (16) of each pair of neighbors under the condition (15) leads to

$$\begin{aligned}(|\delta_{ij}^{(t+1,k)}-\delta_{ij}^{(t,k)}|+|\delta_{ij}^{(t,k)}-\delta_{ij}^{(t-1,k)}|)^2 \\ =[\delta_{ij}^{(t+1,k)}-\delta_{ij}^{(t,k)}-(\delta_{ij}^{(t,k)}-\delta_{ij}^{(t-1,k)})]^2 \\ =(\delta_{ij}^{(t+1,k)}-2\delta_{ij}^{(t,k)}+\delta_{ij}^{(t-1,k)})^2. \qquad \text{(A1)}\end{aligned}$$

This corresponds to the (square of the) discretized second time derivative of $\delta_{ij}^{(t,k)}$ at time t. Thus, each pair of neighbors contributes the "curvature" of $\delta_{ij}^{(t,k)}$ to the CA fluctuation number Ω.

In order to exploit this relation further, we assume that the system under consideration obeys a one-dimensional first-order differential equation at each lattice point. The whole lattice at discrete time steps leads to the "images" $\mathcal{I}(t)$. The system, thus represented as a coupled-map lattice then has the following form:

$$\dot{x}_{ij}(t)=f[x_{ij}(t)]+\xi_{ij}(t)+D\sum_{b\in\mathcal{N}_{ij}}[b(t)-x_{ij}(t)],$$
$$i,j=1\ldots N, \qquad \text{(A2)}$$

where f in general is a nonlinear function, $\xi_{ij}(t)$ is a spatially and temporally incoherent noise and D is the diffusion constant. This equation is solved by

$$x_{ij}(t)=\int_0^t \dot{x}_{ij}(t')dt'-x_{ij}(0). \qquad \text{(A3)}$$

The contribution, Eq. (A1), to the fluctuation number in this formulation is $(t\pm 1\rightarrow t\pm\Delta t)$,

$$
\begin{aligned}
&[\{x_{ij}(t+\Delta t)-x_{ij}^{(k)}(t+\Delta t)\}-2\{x_{ij}(t)-x_{ij}^{(k)}(t)\}+\{x_{ij}(t-\Delta t)-x_{ij}^{(k)}(t-\Delta t)\}]^2 \\
&\quad=\left[\left(\int_t^{t+\Delta t}-\int_{t-\Delta t}^{t}\right)\left\{f[x_{ij}(t')]+D\sum_{b\in\mathcal{N}_{ij}}[b(t')-x_{ij}(t')]-f[x_{ij}^{(k)}(t')]-D\sum_{c\in\mathcal{N}_{ij}^{(k)}}[c(t')-x_{ij}^{(k)}(t')]\right\}dt'\right. \\
&\qquad\left.+\int_t^{t+\Delta t}\{\xi_{ij}(t')-\xi_{ij}^{(k)}(t')\}dt'-\int_{t-\Delta t}^{t}\{\xi_{ij}(t')-\xi_{ij}^{(k)}(t')\}dt'\right]^2 \\
&\quad=\left[\left(\int_t^{t+\Delta t}-\int_{t-\Delta t}^{t}\right)g(t')dt'+\left(\int_t^{t+\Delta t}-\int_{t-\Delta t}^{t}\right)\{\xi_{ij}(t')-\xi_{ij}^{(k)}(t')\}dt'\right]^2 \\
&\quad=[\Delta t\cdot[g(t_2)-g(t_1)]+\eta_{ij}^{(k)}(t,\Delta t)]^2, \qquad \text{(A4)}
\end{aligned}
$$

where $g(t)$ and $\eta_{ij}^{(k)}(t,\Delta t)$ are summing up the deterministic and stochastic part, repectively. The mean value theorem was used, which implies continuity of $g(t)$ ($t_1\in[t-\Delta t,t]$,$t_2\in[t,t+\Delta t]$). With a small Δt in comparison to the time scale of the variation of $g(t)$, the deterministic part vanishes and the stochastic one remains to be registered by $\Omega(t)$. Assuming further a Gaussian white noise $\xi_{ij}(t)$ with

$$
\begin{aligned}
\langle\xi_{ij}(t)\rangle&=0, \\
\langle\xi_{ij}(t)\xi_{kl}(t')\rangle&=\delta_{ik}\delta_{jl}\delta(t-t')\sigma^2 \qquad \text{(A5)}
\end{aligned}
$$

gives for $\eta_{ij}^{(k)}(t,\Delta t)$,

$$
\begin{aligned}
\langle\eta_{ij}^{(k)}(t,\Delta t)\rangle&=0, \\
\langle\eta_{ij}^{(k)}(t,\Delta t)\,\eta_{mn}^{(l)}(t,\Delta t)\rangle&=\delta_{im}\delta_{jn}\delta_{kl}\delta(t-t')4\sigma^2\Delta t. \qquad \text{(A6)}
\end{aligned}
$$

Neglecting the filter term in Eq. (15) results in the approximation,

$$
\Omega(t)\approx\frac{1}{N^2}\sum_{ij}\frac{1}{|\mathcal{N}_{ij}|}\sum_{k=1}^{|\mathcal{N}_{ij}|}[\eta_{ij}^{(k)}(t,\Delta t)]^2\approx 4\sigma^2\Delta t, \qquad \text{(A7)}
$$

where a large N is sufficient for the second equality. Thus, the CA fluctuation number $\Omega(t)$ is proportional to the variance of the initial noise and, therefore, an excellent measure of the noise content of the observed dynamics. An important necessity for the first approximation in Eq. (A7) is a gap between the time scales of the initial noise and of the deterministic part placing Δt in between to account for the noisy contribution.

[1] L. Gammaitoni, P. Hänggi, P. Jung, and F. Marchesoni, Rev. Mod. Phys. **70**, 223 (1998).

[2] K. Wiesenfeld and F. Moss, Nature (London) **373**, 33 (1995).

[3] F. Moss, Stochastic resonance: looking forward, in *Self-organized Biological Dynamics and Nonlinear Control*, edited by J. Walleczek (Cambridge University Press, Cambridge, 2000), pp. 236–256.

[4] P. Jung and G. Mayer-Kress, Phys. Rev. Lett. **74**, 2130 (1995).

[5] P. Jung, A.H. Cornell-Bell, F. Moss, K. Sadar, J. Wang, and K. Showalter, Chaos **8**, 567 (1998).

[6] J.E. Levin and J.P. Miller, Nature (London) **380**, 165 (1996).

[7] D. Nozaki, D.J. Mar, P. Grigg, and J.J. Collins, Phys. Rev. Lett. **82**, 2402 (1999).

[8] M.-Th. Hütt, *Datenanalyse in der Biologie* (Springer, Heidelberg, 2001).

[9] B. Jähne, *Practical Handbook on Digital Image Processing for Scientific Applications* (CRC-Press, Boca Raton, 1997).

[10] G.K. Harkness, J. Lega, and G.-L. Oppo, Physica D **96**, 26 (1996).

[11] H. Herzel, Curr. Top. Acoust. Res. **2**, 17 (1998).

[12] S. Ninagawa, M. Yoneda, and S. Hirose, Physica D **118**, 49 (1998).

[13] H.G. Jones, Plant Cell Envir. **22**, 1043 (1999).

[14] T. Lawson and J. Weyers, J. Exp. Bot. **50**, 1381 (1999).

[15] *Measures of Spatio-Temporal Dynamics*, edited by A.M. Albano, P.E. Rapp, N.B. Abraham, and A. Passamante (Elsevier Science B.V., Amsterdam, 1996).

[16] S. Wolfram, Nature (London) **311**, 419 (1984).

[17] Y. Bar-Yam, *Dynamics of Complex Systems* (Addison-Wesley, Reading, MA, 1997).

[18] G.B. Ermentrout and L. Edelstein-Keshet, J. Theor. Biol. **160**, 97 (1993).

[19] M. Markus, A. Czajka, D. Böhm, T. Hahn, T. Schulte, and A. Ribeiro, in *Cellular Automata and Complex Systems*, edited by E. Goles and S. Martinez (Kluwer Academic Publishers, Dordrecht, 1999).

[20] M.-Th. Hütt and R. Neff, Physica A **289**, 498 (2001).

[21] N.G. van Kampen, *Stochastic Processes in Physics and Chemistry–Revised and Enlarged Edition* (Elsevier, Amsterdam, 1992), pp. 55–58.

[22] H. Busch and M.-Th. Hütt, Int. J. Bifurcation Chaos Appl. (to be published).

[23] Y. Zhou and P. Jung, Europhys. Lett. **49**, 695 (2000).

[24] B. Braaksma and J. Grasman, Physica B **68**, 265 (1993).

[25] H. Busch and F. Kaiser, Acta Phys. Pol. B **31**, 1143 (2000).
[26] T. Tsujikawa, T. Nagai, M. Mimura, R. Kobayashi, and H. Ikeda, Jpn. J. Appl. Math. **6**, 341 (1989).
[27] E.E. Sel'kov, Eur. J. Biochem. **4**, 79 (1968).
[28] J. Garcia-Ojalvo and J.M. Sancho, *Noise in Spatially Extended Systems* (Springer, New York, 1999).
[29] U. Rascher, M-T. Hütt, K. Siebke, B. Osmond, F. Beck, and U. Lüttge, Proc. Natl. Acad. Sci. U.S.A. **98**, 11 801 (2001).